Journal of Applied Sciences Research 4(12): 2089-2097, 2008

Geologic Tieing of Undefinable Tops Through the Construction of Synthetic Seismograms for Some Wells Selected in Al Amal Field, Suez Gulf, Egypt

Elhamy A. Tarabees

Geology Department, Faculty of Science, Alexandria University, Egypt.

Abstract: The first problem for the geophysicist is to tie the depth derived from well logs with the seismic time scale. Therefore, the present study is a trial to construct synthetic seismograms for four wells in Al Amal field, Gulf of Suez, Egypt. These wells are Amal -9, Amal -10, Amal -11 and Amal -12. In each of these wells, a version of synthetic seismogram is resulted. These geograms were established using Ricker wavelet, normal SEG polarity, zero-phase and the frequency band pass filters (3, 6 - 30, 40) Hz., as well as the primaries without transmission loss. Moreover, the geograms are used to study the vertical changes in the reflection characteristics of the comparable stratigraphic units. The cyclic nature of sedimentation among the studied formations played an important role in the magnitudes and polarities of the reflectivity of the included boundaries.

Key wards: synthetic seismogram, seismic reflection, oil exploration, Gulf of Suez

INTRODUCTION

The previous studies show that, gravity cores can disrupt the sediment[12,20] and the use of synthetic seismograms can depict the various disruptions that occurred[15]. When a synthetic seismogram is generated, it can be compared to the seismic profile at the location the core was recovered, and the synthetic trace should align with the horizons displayed in the seismic profile. If they do not align, objectively manipulating the variables used (bulk density and velocity) to create a synthetic seismogram to improve the corroboration and indicate what types of disruption (gaps, expansion and compaction) occurred during the coring process.

A study by Brew and Mayer[5] used synthetic seismograms to observe with sediment horizons in the Hatteras Outer Ridge in the western North Atlantic. In this study, the physical properties and seismic profiles were accumulated to create synthetic seismograms and to gain a better understanding of abyssal mud waves[5]. They determined that, the physical properties have been altered when the sediment was removed from its in-situ position. They accounted for porosity rebound by objectively manipulating the density and velocity variables. Brew and Meyer[5] determined the proper density and velocity profiles by developing a synthetic seismogram (using adjusted density and velocity variables), that has the strongest correlation with the seismic profile. They found that, the original densities determined on the board of the ship were erroneously high due to over compaction and the calculated velocities also are too high. After corrections, the synthetic seismograms demonstrated a strong correlation between the seismic data and the cores physical properties.

Flood and Shor[8] used synthetic seismograms to correlate the observed seismic horizons with the carbonate peaks within the sediment. Since the seismic data matches the physical property data, it validates both data sets. Ultimately, Flood and Shor[8] suggested that, geological data can be directly correlated to seismic profiles and still provide concrete evidence of specific reflectors, even in cases where physical property data is lacking. Manley[15], in the Gerlache Straight, correlated seismic reflectors within large sediment deposits after taking coring disruption into account through the use of synthetic seismograms. Her study indicates that, the high water content in cores can result in heavy compaction and therefore under sampling. Manley[15] agrees with Hamilton[12] in that, sediment may elastically rebound and increase its volume when dense ocean sediments are removed from the ocean floor. Controls such as stretching and compressing of the density profile can be used to account for the over compaction and elastic rebound of sediment[15]. The synthetics reveal that, sedimentation rates and paleoclimate interpretations from uncalibrated cores may be inaccurate due to the excessive disturbances of the sediment. The creation of synthetic seismograms proves to be an effective tool in understanding the core disruption and determining a correct depth profile. The synthetic seismograms were also used to better explaining the seismic horizons and showed that, lithology changes, in particular sand/ash

Corresponding Author: Elhamy Tarabees, Geology Department, Faculty of Science, Alexandria University, Egypt. Email: etarabees@yahoo.com

layers, to be the dominant cause of the reflectors[17]. Accordingly, this subject was studied theoretically and practically by many authors. Among these: Butterworth[6,1,14,18,22,11,23,16,19,13,10,21,2,3] and others.

Geologic Setting: The Gulf of Suez covers an area of about 25000 Km^2. It extends along a Northwest trend from latitude 27° 30' to 30° 00' N. The Amal field area is about 27 Km^2 in the off-shore, southern part of the Gulf of Suez basin (Fig. 1). It is located on a NW - SE faulted monocline, which has a SW dip, plunging NW and SE, sealed by the clysmic faults and capped by the Middle - Late Miocene evaporites. In view of the Amal field history, the main reservoir is the Miocene sandstone of Kareem and Rudeis Formations, while oil shows are encountered in the pre-Miocene reservoirs, which are not yet well explored.

Stratigraphically, the basement is unconformably overlain by the Paleozoic to Early Cretaceous sediments (Nubia Sandstone sequence), which are in turn unconformably overlain by a complete sequence of strata ranging in age from Cenomanian to Middle Eocene. These strata are subdivided into seven rock units, namely Raha, Wata, Matulla, Sudr, Esna, Thebes and Samalut Formations. The Pre-Miocene sequence is intruded in some wells by basaltic dykes of probable Oligocene age. The Samalut Formation is unconformably overlain by Abu Zenima Formation, which is overlain by Nukhul, Rudeis and Kareem Formations, of the Early to Middle Miocene age. The Early and Middle Miocene clastics (mostly shale) of Rudeis and Kareem Formations are well developed in Abu Rudeis-Sidri Field. Two to three evaporite beds were recorded at the base of Kareem Formation. The Middle to Late Miocene rocks include three formations: Belayim, South Gharib and Zeit Formations. The Post-Miocene sequence in Abu Rudeis-Sidri Field is composed mainly of sandstone and clay sequence. However, the detailed stratigraphic subdivisions of the Gulf of Suez of Egypt are shown in Fig. (2).

Structurally, the structural setting in the Gulf of Suez province is complicated and dissected by a complex pattern of faults. Some of these faults are normal faults and trending parallel to the gulf coast, while the others are strike-slip elements and trending traverse to the gulf shore. The result of such intersection is the fracturing of the Gulf of Suez section into numerous fault blocks (horsts and grabens) with variable throws and dimensions. Abu Rudeis-Sidri Field structure is located in the neighborhood of major fault transfer zones of : 1) W. Feiran - G. Nezzazat bounding fault (trending NNW to NW), 2) G. Nezzazat - W. Baba bounding fault (trending NNE to NS), and 3) W. Baba - Nukhul block bounding fault (trending NW oblique)

MATERIALS AND METHODS

Available Data: The borehole compensated sonic logs (BHC) for the four given wells represent the basic source of velocities, while the formation density compensated logs (FDC) of the same wells exhibit the source of densities. Also, the composite logs of these wells are available to define their chrono-stratigraphic subdivisions, the lithologies of their rock units and the depths of their formational tops.

Theory of Synthetic Seismograms Construction: When a plane seismic wave strikes a plane interface existed between two different rock materials, it will be partially reflected and partially transmitted. For the case of normal incidence[16], the ratio of the amplitudes of the reflected and incident waves, which is known as the reflection coefficient, can be calculated as follows: If a sinusoidal wave of frequency, incident at the interface (Fig. 3), it will be described by the equation:

$$\xi_I = \xi\, I \exp 2\pi / v\, (t - x / c_1) \quad (1)$$

where: ξ_I is the displacement of the propagated seismic waves.

t is the time arrival of these waves.
x is the distance measured perpendicular to the interface.
c is the velocity of propagation.
v is the frequency of the propagated waves.

The mathematical form of the reflected and transmitted waves will be:

$$\xi_R = \xi\, R \exp 2\pi / v\, (t - x / c_1) \quad (2)$$

and

$$\xi_T = \xi\, T \exp 2\pi / v\, (t - x / c_1) \quad (3)$$

At the interface, both the displacement and pressure must be continuous. Therefore, if the interface is at x = 0, the displacement conditions can give:

$$\xi_I + \xi_R = \xi_T \quad (4)$$

Re-collecting this situation, the pressure is given by:

$$\Psi \cdot \frac{\partial \xi}{\partial x} \quad (5)$$

where: Ψ is the axial modulus.

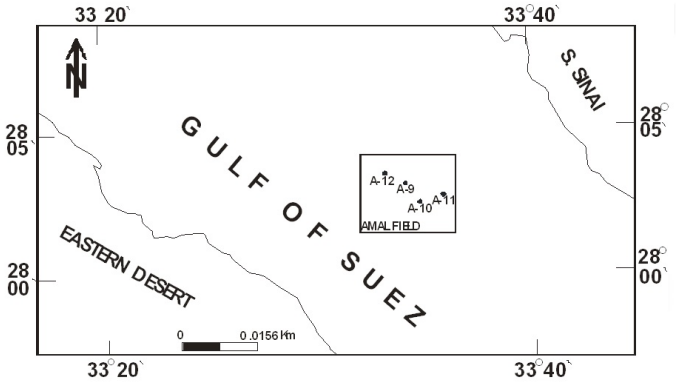

Fig. 1: Location Map of the study area.

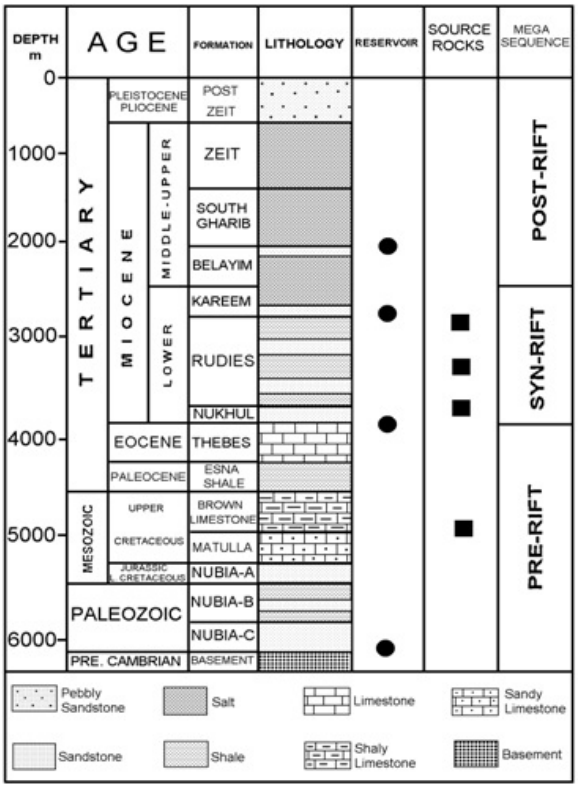

Fig. 2: Generalized Stratigraphic Column of the Gulf of Suez (After EGPC, 1996).

Then, the pressure conditions can give:

$$-\frac{\Psi_1 \cdot \xi_I}{c_1} + \frac{\Psi_1 \cdot \xi_R}{c_1} = -\frac{\Psi 2 \cdot \xi_T}{c_2} \qquad (6)$$

By combining equations (4) and (6), the integrated conditions can give:

$$\frac{\xi_R}{\xi_I} = \frac{\Psi_1 / c_1 - \Psi 2 / c_2}{\Psi_1 / c_1 + \Psi 2 / c_2} \qquad (7)$$

But; $c = \sqrt{\Psi / \rho}$ or $\Psi / c = \rho c$

Therefore, $\frac{\xi_R}{\xi_I} = \frac{\rho_1 c_1 - \rho_2 c_2}{\rho_1 c_1 + \rho_2 c_2}$ (8)

which is the required reflection coefficient.

Moreover, if the acoustic impedance is defined by the relation; (r = ρc), where: ρ is the density and c is

the velocity; the reflected wave will be observed whenever there is a change of the acoustic impedance at the interface.

Therefore, the reflection coefficient for the pressure amplitudes will be given by:

$$\frac{P_R}{P_I} = \frac{r_2 - r_1}{r_2 + r_1} \quad (9)$$

where:

P_I is the pressure amplitude of the incident wave.
P_R is the pressure amplitude of the reflected wave.

Thus, there will be a phase reversal, which means a negative coefficient, if the incident ray is in the higher impedance material. At inclined incidence, the derivation of a general formula is difficult, because of a partial conversion to the shear waves can be occurred. Generally, the reflection coefficient increases as the angle of incidence increases and becomes large in the vicinity of the critical angle. In the seismic reflection practice, the data is obtained only at near-normal incidence, while the data at inclined incidence would be useful, where there is no difference of acoustic impedances across an interface, because c and ρ change normally in opposite directions.

Added, the part of seismic energy that not reflected at the interface is transmitted into the second medium, undergoing reflection at the interface. The angle of seismic reflection is related to the angle of incidence by Snell's law:

$$\text{Sin } r / \text{Sin } i = c_2/c_1 \quad (10)$$

where:
c_1 is the velocity on the incident ray side.
c_2 is the velocity on the refracted ray side.
I is the angle of incidence.
r is the angle of refraction.

Finally, the process of production of the synthetic seismograms involves the display of the convolution product of the reflection coefficient with a suitable zero or minimum phase wavelet of frequency response similar to that of the records in the vicinity of the considered area. Cartoon of convolution equation: RC * source signature = synthetic seismogram[4,15] is shown in fig. (4). Ricker wavelets are often used to generate synthetic seismic records (Fig. 5). To ensure a reasonable match, the frequency of the synthetic Ricker wavelet used is generally estimated on the basis of a qualitative and/or quantitative analysis of the acquired field reflection seismic data. If the field seismic data have been processed and transformed into zero-phase equivalent, a zero-phase synthetic Ricker wavelet is often used. If the field seismic data were acquired using an impulsive source - but have not been transformed into zero-phase equivalent during processing, a minimum-phase synthetic Ricker wavelet is often used. The polarity of the synthetic wavelet employed is a function of the polarity of the interpreted field seismic data. Some interpreters prefer to work with normal polarity reflection seismic data; others prefer to work with reverse polarity data (Fig. 5).

Procedure of Synthetic Seismogram Construction: Based on the previously mentioned theoretical background and method followed in the generation of geograms of the studied wells, the initial logs (sonic and density) are digitized and the wavelet parameters are specified for each well and fed into the system of reflection coefficient computation, reflection spikes presentation and reflectivity series convolution with the selected filter operator to produce the wanted synthetic seismograms. An Interactive Geoquest Computer (IES-synthetic seismogram programs) has been used to create those synthetic seismograms. System interaction is achieved with a combination of menus and graphical displays. The set of synthetic seismograms application menus is presented in parallel with discussions of the functions controlled by these menus. The final graphics screen display includes the primitive logs (velocity and density), intermediate results (acoustic impedance) and the final displays of synthetic seismograms. These geograms layouts are presented using the electrostatic work-stations or thermal plotters.

RESULTS AND DISCUSSION

Application in the Study Area: The synthetic seismogram of Amal -9 well (Fig. 6) is created using Ricker wavelet of frequency (3 - 30) Hz with normal polarity and zero - phase in the form of primaries without transmission loss. This version shows the largest reflectivities for the Hammam Faraun and Feiran Members as well as Kareem, Thebes and Esna Shale Formations boundaries and the least reflectivities for Kareem and Rudeis Formations contacts.

The display of the synthetic seismogram of Amal -10 and Amal -11 wells (Figs. 7 & 8) are generated using Ricker wavelet of frequency (6 - 40) Hz with normal SEG polarity and zero-phase in the form of the primaries without transmission loss. The versions reveal the largest retlectivities for Belayim and Kareem Formations, Markha Member and Rudeis Formation contacts, as well as the least reflectivities for Nukhul and Thebes Formations boundaries.

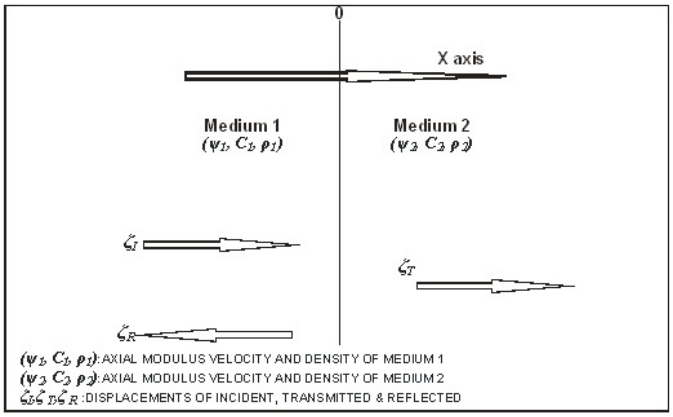

Fig. 3: Calculation of Reflection Coefficient at Normal Incidence (Mc Quillin, 1980)

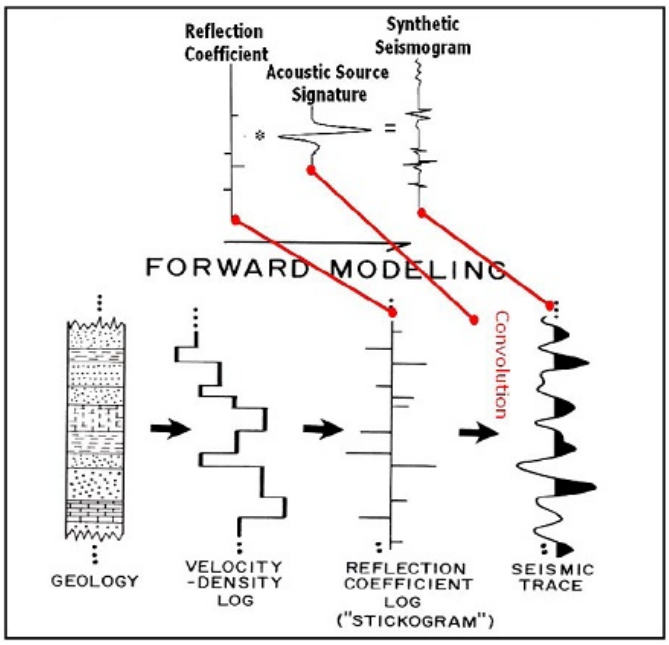

Fig. 4: Cartoon of Convolution Equation: Rc* Source Signature = Synthetic Seismogram (Adapted from Bissell, 1993 and Manley, 2004).

Also, the synthetic seismogram of Amal -12 well (Fig. 9) is created using Ricker wavelet of frequency (3 - 30) Hz with normal polarity and zero - phase. This version delineates the largest reflectivities for South Gharib, Belayim and Kareem Formations Markha Member and Rudies Formation boundaries and the least reflectivities for Rudeis and Nukhul Formations contacts.

In conclusion, the contacts characterized by the largest magnitudes in reflectivity are normally represented on the seismic sections with the maximum clearness of their events and vice versa for the lowest magnitudes. The parts of the boundaries characterized by positive reflectivity signs are illustrated on the seismic sections as black peaks, while those implicated by negative polarities appeared as white troughs. This indicates that, the change of the polarity of the seismic events is essentially associated with comparable variation of the rock types on both sides of the considered contacts.

Finally, it has been shown from the construction of the four synthetic seismograms of the studied wells with the various parameters that, Ricker wavelet of (3,6 -30,40)Hz frequencies, normal SEG polarity and zero-phase is the best wavelet type and parameters used for correlation of the synthetic seismograms with the real seismic data of the area under investigation. Time shift may exist between the geogram data and the field data

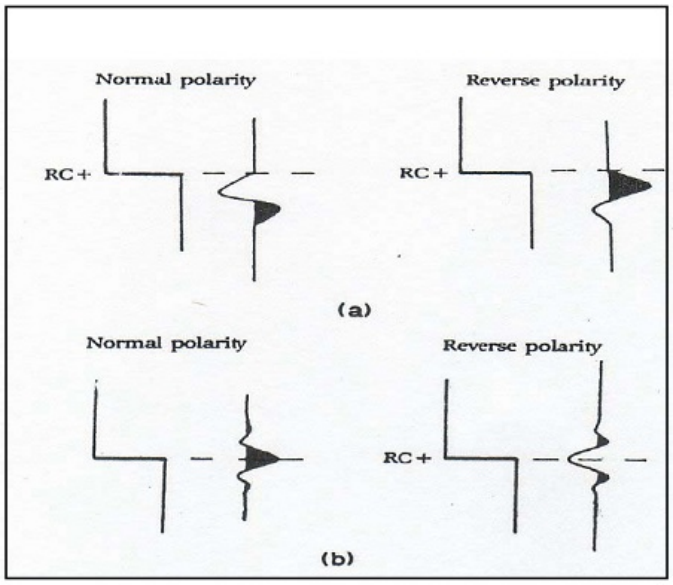

Fig. 5: Polarity Conventions. For a Positive Reflection (Increase in Acoustic Impedance), a Minimum Phase Wavelet (5a) Begins with a down Kick, and (5b) the Center of a Zero-phase Wavelet Is a Peak. (After Sheriff, 1995.)

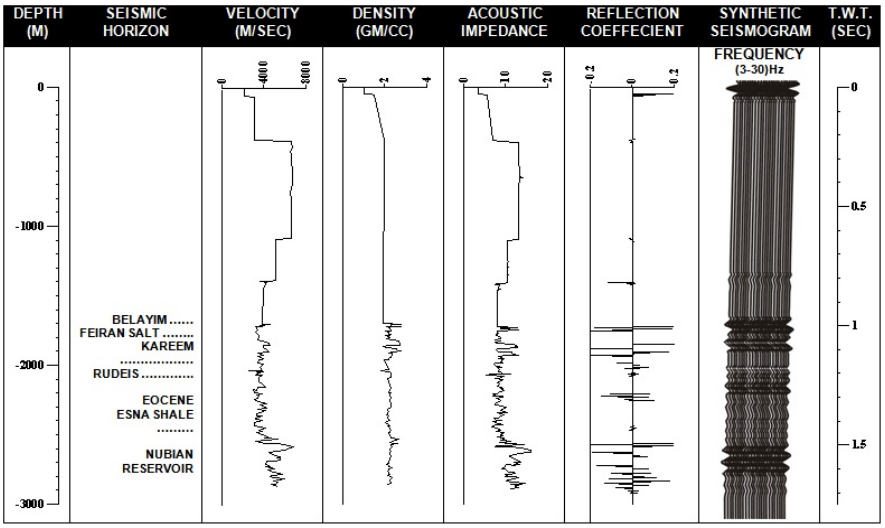

Fig. 6: Synthetic Seismogram of Amal- 9 Well

due to the fact that, these seismograms are represented without applying the check shots that correct the given sonic times.

Interpretation of the Seismic Sections: From the construction of the four synthetic seismograms of the studied wells with the various parameters that, Ricker wavelet of (3, 6 -30, 40) Hz frequencies, normal SEG polarity and zero- phase is the best wavelet type and parameters used for correlation of the synthetic seismograms with the real seismic data of the area under investigation. The correlation shows a good matching between the synthetic seismograms with the real seismic data recorded at the study area. Fig. (10) is one of these interpreted seismic data with aid of the synthetic seismograms. This seismic profile has NW - SE trend and shows step faults of opposite throws and structural low (graben), all are interrupted by normal faults of opposite throws and different lengths.

Summary and Conclusions: The theory of synthetic seismograms construction is explained. Wavelet parameters including wavelet types, frequency contents, reflection polarities and phase angles are also

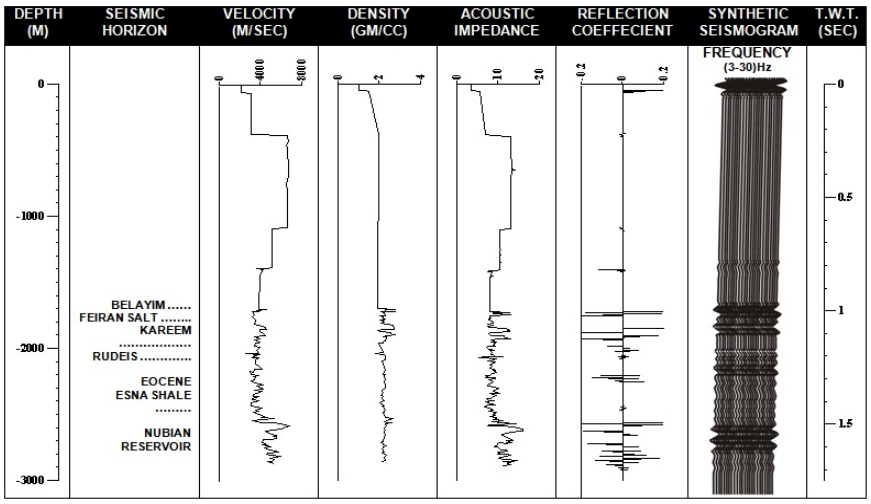

Fig. 7: Synthetic Seismogram of Amal -10 Well

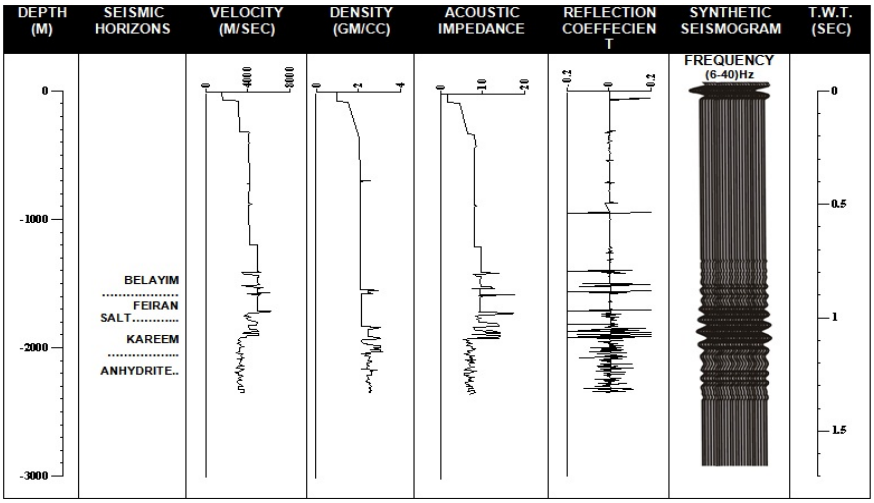

Fig. 8: Synthetic Seismogram of Amal -11 Well

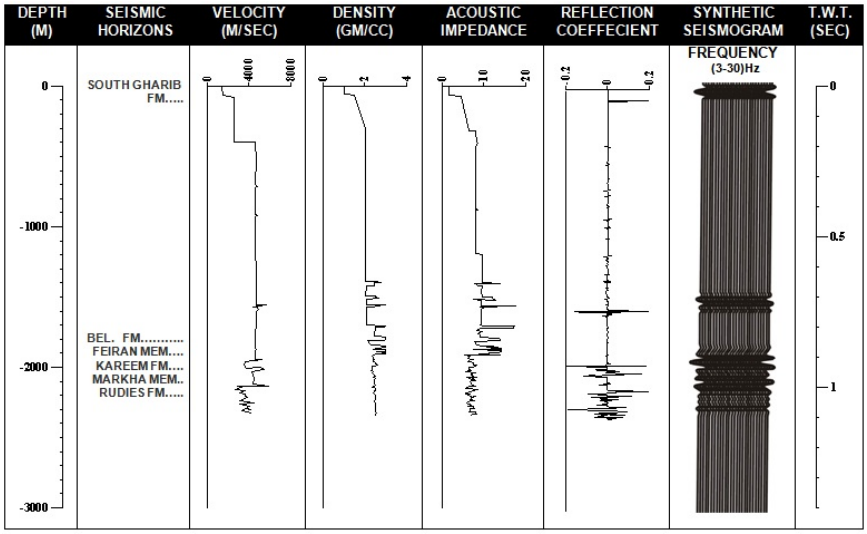

Fig. 9: Synthetic Seismogram of Amal -12 Well

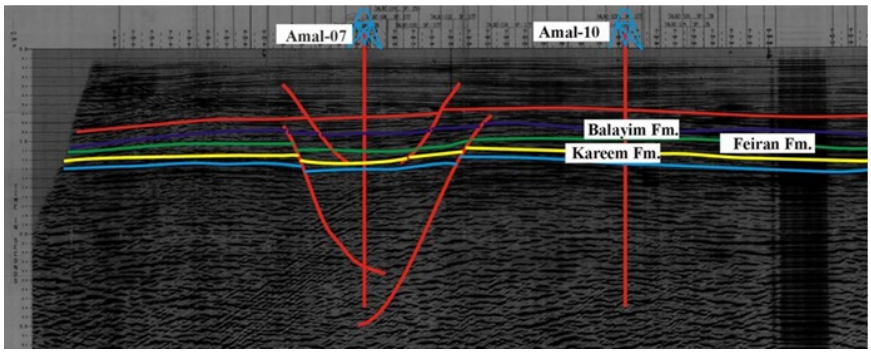

Fig. 10: An Example for an Interpreted Seismic Profile Usingthe Synthetic Seismogram of Amal -10 Well

enumerated. Accordingly, the synthetic seismograms of the four studied wells in the investigated area (Amal-9, Amal-10, Amal-11 and Amal-12) are constructed. For each of these wells, a version of geogram is produced. These versions are established through Ricker wavelet of (3, 6 - 30, 40) Hz frequency band pass, normal SEG polarity and zero-phase in the form of the primaries without transmission loss. These geograms showed the vertical changes in the reflection characteristics of the comparable stratigraphic units. In conclusion, the fore-mentioned parameters of the produced geograms are considered the best wavelet types and characteristics used for correlation of the synthetic seismograms with the real seismic data of the area under investigation.

AKNOWLDEGMENT

The author would like to express about his thanks and gratitude for the Professor Dr. Salah Shebl, Exploration Department, Egyptian Petroleum Research Institute, Egypt**,** for the useful discussions during the data processing and interpretation and reading the manuscript.

REFERENCES

1. Anderson, B. John, 1999. Antarctic Marine Geology. Cambridge University Press, pp: 289.
2. Anstey, N.A., 1960. Attacking the problems of the synthetic seismogrames, Geophys. Prosp.V.B, pp: 242-259.
3. Belknap, F. Daniel and Shipp, Craig, 1991. Seismic stratigraphy of glacial marine units, Maine inner shelf. Glacial marine Sedimentation; Paleoclimatic significance, pp: 137-158.
4. Bissell, M.D., 1993. Synthetic Seismogram Generation: A Study in the Antarctic Peninsula Region. Unpublished Senior Thesis, Middlebury College, Middlebury, Vermont.
5. Brew, S.D., A.L. Mayer, 1998. Modeling of Pliocene-Pleistocene abyssal mud waves using synthetic seismograms. Marine geology, 149: 3-16.
6. Butterworth, S., 1930. On the theory of filter amplifiers wireless. Eng, l: 536-541.
7. EGPC (Egyptian General Petroleum Corporation), 1996. Western Desert, oil and gas fields. EGPC, Cairo, Egypt, pp: 431.
8. Flood, R.D. and A.N. Shor, 1984. Synthetic seismogram generation from sediment composition data - An initial Study in the southwest Brazil Basin. Marine Geology, 58: 263 -274.
9. Ganley, D.C., 1981. A method for calculating synthetic seismograms which include the effects of absorption and dispersion, transmission, 46: 1100 -1107.
10. Gomber, L., 1983. Correlation of attenuation of seismic waves with other petrophysical and lithological properties, Geophysics Transact, 29: 217-228.
11. Hampton, L.D., 1967. Acoustic properties of sediment J. Acoust. Soc. Am., 42: 882 -890.
12. Hamilton, L.E., 1976. Variations of Density and porosity with depth in deep-sea sediments. The J. of Sedimentary Petrology, 40(2): 280 - 300.
13. Kanasewich, E.R., 1981. Time sequence analysis in geophysics 3rd ed., University of Alberta Press, Edmonto, Alberta.
14. Lindapy, J.P., 1960. Elimination of seismic ghost reflections by means of a linear filter, Geophysics, 25: 130-I40.
15. Manley, P.L., 2004. Synthetic seismograms and acoustic facieses of the Anvord and Schollaert Drifts: Antarctic Peninsula, Antarctica Peninsula Climate Variability: History Causes and Impacts, Cambridge.
16. Mcquillin, M., A. Bacon and W. Barclay, 1980. An introduction seismic interpretation; Mc Graw-Hill Co., U.S.A., pp: 267.

17. Michalchuk, R.B., 2006. Synthetic Seismograms and Physical Properties Generated from Sediments in Maxwell Bay, Antarctica - A Study of Climate History. Senior Thesis, Middlebury College, Middlebury, Vermont, 05753.
18. Schoenberger, M. and F.K. Levin, 1979. The effect of subsurface sampling on one-dimensional synthetic seismograms, Geophysics, 44: 813-822.
19. Sheriff, R.E. and L.P. Geldart, 1995. Exploration Seismology, second edition: Cambridge University Press, pp: 592.
20. Skinner L.C. and I.N. McCave, 2003. Analysis and modeling of gravity-and piston coring based on soil mechanics. Marine Geology, 199: 181-204.
21. Syvitski, J.P.M., D.C. Burrell and J.M. Skei, 1987. Fjords: Processes and Products, Springer-Verlag, New York, pp: 379.
22. Trorey, A.W., 1962. Theoretical seismograms with frequency and depth dependent absorption, Geophysics, 27: 766-785.
23. White, J.E., 1975. Computed seismic speeds and attenuation in rocks, Geophysics, 40: 244 - 252.